AMERICAN SOCIETY FOR MICROBIOLOGY | Journal of Bacteriology®

MEETING PRESENTATION

Depletion of Glucose Activates Catabolite Repression during Pneumonic Plague

Jeremy T. Ritzert,[a] Wyndham W. Lathem[a]

[a]Department of Microbiology-Immunology, Northwestern University Feinberg School of Medicine, Chicago, Illinois, USA

ABSTRACT Bacterial pathogenesis depends on changes in metabolic and virulence gene expression in response to changes within a pathogen's environment. The plague-causing pathogen, *Yersinia pestis*, requires expression of the gene encoding the Pla protease for progression of pneumonic plague. The catabolite repressor protein Crp, a global transcriptional regulator, may serve as the activator of *pla* in response to changes within the lungs as disease progresses. By using gene reporter fusions, the spatial and temporal activation of the *crp* and *pla* promoters was measured in a mouse model of pneumonic plague. In the lungs, *crp* was highly expressed in bacteria found within large aggregates resembling biofilms, while *pla* expression increased over time independent of the aggregated state. Increased expression of *crp* and *pla* correlated with a reduction in lung glucose levels. Deletion of the glucose-specific phosphotransferase system EIIBC (PtsG) of *Y. pestis* rescued glucose levels in the lungs, resulting in reduced expression of both *crp* and *pla*. We propose that activation of *pla* expression during pneumonic plague is driven by an increase of both Crp and cAMP levels following consumption of available glucose in the lungs by *Y. pestis*. Thus, Crp operates as a sensor linking the nutritional environment of the host to regulation of virulence gene expression.

IMPORTANCE Using *Yersinia pestis* as a model for pneumonia, we discovered that glucose is rapidly consumed, leading to a catabolite-repressive environment in the lungs. As a result, expression of the gene encoding the plasminogen activator protease, a target of the catabolite repressor protein required for *Y. pestis* pathogenesis, is activated. Interestingly, expression of the catabolite repressor protein itself was also increased in the absence of glucose but only in biofilms. The data presented here demonstrate how a bacterial pathogen senses changes within its environment to coordinate metabolism and virulence gene expression.

KEYWORDS *Yersinia pestis*, plague, Pla, catabolite repression, Crp, PtsG, glucose

Yersinia pestis, the agent of plague, causes a rapidly progressing pneumonia resulting in death if the infection is untreated (1). Pneumonic plague is a biphasic infection, characterized by an initial quiescent state giving way to a severe inflammatory phase 36 to 48 h postinfection (hpi) (2). This phase shift corresponds with recruitment of neutrophils to the lungs, leakage of serum into the alveolar space, and the onset of disease symptoms (3). During this time, *Y. pestis* proliferates within the alveolar space up to 10^9 CFU per lung and disseminates from the lungs into the bloodstream. To link changing gene expression levels during these phases, transcriptional profiles of *Y. pestis* during growth in plasma, the bubo, and the lungs have been analyzed (4–6). Yet little is known about how *Y. pestis* adapts to the changing nutritional environment and regulates virulence gene expression within the lung space as the pneumonia progresses.

The plasminogen activator protease, *pla*, required for pneumonic and bubonic

Received 6 December 2017 **Accepted** 11 March 2018

Accepted manuscript posted online 19 March 2018

Citation Ritzert JT, Lathem WW. 2018. Depletion of glucose activates catabolite repression during pneumonic plague. J Bacteriol 200:e00737-17. https://doi.org/10.1128/JB.00737-17.

Editor Victor J. DiRita, Michigan State University

Address correspondence to Jeremy T. Ritzert, jeremy.ritzert@northwestern.edu.

plague (7, 8), manipulates programmed cell death pathways and deregulates the host fibrinolysis pathways (9). Not only does Pla activate host plasminogen into plasmin, but it also inactivates inhibitors of plasmin activation, α_2-antiplasmin and plasminogen activation inhibitor 1 (PAI-1) (10, 11). In the absence of catalytic activity of Pla, *Y. pestis* fails to proliferate in the lungs and poorly disseminates into the bloodstream (7). The necessity of Pla for *Y. pestis* to cause a successful pneumonia and develop pandemic potential has been well studied (12), but its control during the onset of infection and in response to the evolving lung environment is less understood.

Transcription of the *pla* gene is known to shift at the transition of the lung environment to a severely inflammatory state 36 to 48 hpi. *In vitro*, *pla* gene expression is dependent on the catabolite repressor protein, Crp (13, 14). Crp is a global regulator found in many species of gammaproteobacteria. When bound to cyclic AMP (cAMP), it activates or represses expression of hundreds of genes in *Yersinia* spp. (15). Levels of cAMP are regulated by the activities of the phosphotransferase system (PTS) and adenylate cyclase (16). EIIBC subunits of the PTS, such as PtsG for glucose, transport sugar molecules across the inner membrane and transfer a phosphate from the EIIA subunit onto the transported substrate. As the extracellular concentration of glucose or other PTS substrates decreases, the concentration of phosphorylated EIIA in cells increases and thereby activates adenylate cyclase to generate cAMP from ATP. Binding of cAMP is required for Crp dimerization and DNA binding activities, allowing cAMP-Crp to activate genes for metabolism of alternative carbon sources (17).

Crp-regulated genes are known virulence determinants in many pathogenic organisms, revealing that virulence is linked to the nutritional status of the surrounding environment (18). In *Yersinia* spp., in addition to regulation of *pla*, Crp regulates expression of genes encoding the type III secretion system and its effectors (19), the anti-phagocytic capsule F1, and hundreds of other protein-coding genes and small noncoding RNAs (sRNAs) (20, 21). In addition, Crp has been suggested to regulate biofilm formation in *Y. pestis* indirectly and with CsrA (22, 23). In contrast to expression in *Escherichia coli*, expression of *crp* itself in *Y. pestis* is not directly auto-regulated (24, 25) but is regulated by the PhoP response regulator (26). The sRNA chaperone Hfq is also required at the *crp* 5′ untranslated region (UTR) for protein translation, suggesting a role for sRNAs in regulation of *crp* (13).

Because Crp and many of its targets are required for virulence, we hypothesized that Crp may critically control virulence gene expression following the transition to the inflammatory phase of infection in response to changes within the lung environment. We observed that at 72 hpi the concentration of glucose was significantly reduced due to consumption by *Y. pestis*. Activity at the *crp* promoter increased during this time within large, biofilm-like aggregates, while activity of the *pla* promoter was increased over time. Deletion of the gene encoding the EIIBC glucose-specific transporter, PtsG, from *Y. pestis* prevented glucose depletion in the lungs of infected mice and inhibited activity of *crp* and *pla* promoters. These data support a model in which *Y. pestis* adapts its virulence gene expression due to changes in its metabolism and sensing of glucose availability through Crp and catabolite repression during pneumonia progression.

RESULTS

Glucose is depleted from the pulmonary compartment during pneumonic plague. *In vitro* studies indicate that catabolite repression controls expression of essential virulence factors of *Y. pestis*. To determine if glucose concentrations change during pneumonic plague, the concentration of glucose was measured in the bronchoalveolar lavage fluid (BALF) of intranasally infected mice at 24, 48, and 72 hpi. The concentration of glucose in the BALF dropped from 25 to 30 μg/ml in uninfected lungs to $<$5 μg/ml in infected lungs at 72 hpi (Fig. 1A). In addition to the $>$5-fold decrease in the concentration of lung glucose, the glucose concentration measured in the blood of infected mice was also reduced 2-fold at 72 hpi (Fig. 1B).

To monitor blood leakage into lung, the same BALF samples were used for measuring albumin. Serum albumin increased more than 60-fold, from 80 μg/ml in mock-

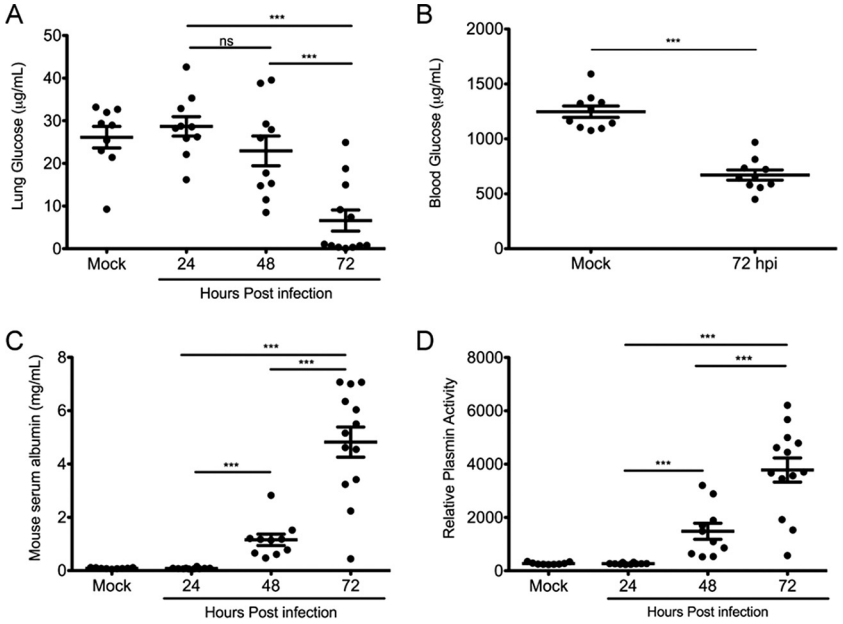

FIG 1 Available glucose in the lungs decreases as the pneumonia progresses. (A) Concentration of glucose in BALF recovered from the lungs of mock (PBS)-infected or *Y. pestis*-infected mice at 24, 48, and 72 hpi. (B) Concentration of glucose in the serum of infected mice at 72 hpi. (C) Concentration of mouse serum albumin in BALF of mock- and *Y. pestis*-infected mice measured by ELISA. (D) Relative plasmin activity in BALF from mock- and *Y. pestis*-infected mice measured by a plasmin activity assay. Data are combined from two independent infections with mock-infected and 24- and 48-h-infected mice ($n = 5$) and 72-h-infected mice ($n = 10$). Error bars represent the means and standard errors of the means. ***, $P < 0.001$; ns, not significant (one-way ANOVA with Bonferroni multiple-comparison test for panels A, C, and D and Student's *t* test for panel B).

infected animals to more than 5 mg/ml in infected animals, at 72 hpi (Fig. 1C). Thus, glucose levels in lung decline even as glucose-rich blood leaks into the BALF.

Finally, the activity of Pla can be measured indirectly by measuring the amount of plasmin in the BALF as Pla activates plasminogen into plasmin. Relative plasmin activity increased significantly between 24 and 48 hpi and further increased at 72 hpi, indicative of continued activation of plasminogen by Pla (Fig. 1D). These data suggest that *Y. pestis* depletes glucose from the lung space despite increased permeability of the lungs. This may trigger catabolite repression control of virulence gene expression as the infection progresses.

Activity at the *crp* promoter is increased within large bacterial aggregates in the lungs. Activity at the *crp* promoter could increase in response to the decline in glucose levels during later stages of infection. Because of the complexity of the lung structure, the environment may not be homogenous across *Y. pestis*-infected lungs, and thus altered expression of *crp* may be spatially distinct. Thus, gene expression was monitored *in situ*. A green fluorescent protein (GFP) promoter fusion containing the *crp* promoter was integrated into the Tn*7* site of *Y. pestis* containing the pGEN-RFP plasmid for constitutive production of red fluorescent protein (RFP) to make bacteria detectable by fluorescence. Cross sections of lungs from mice infected with these strains were then imaged by confocal microscopy. The ratio of GFP to RFP in bacterial cells was used to determine any spatial or temporal increases in promoter activity as a surrogate for gene expression in bacteria within the lungs. *Y. pestis*-containing lesions could be reliably captured in infected mice at 36 hpi, before the bacteria proliferated to the order of 10^8 to 10^9 CFU at 72 hpi (Fig. 2A). As a negative control, mice were infected with *Y. pestis* harboring a fusion containing the constitutive *tetO* promoter fused to *gfp*. Infections with this strain (and other reporter strains) caused lethal lung infections, with bacterial burdens and pathologies in the lungs similar to those of infection with wild-type strains (see Fig. S1 in the supplemental material). No spatial or temporal changes in the ratio

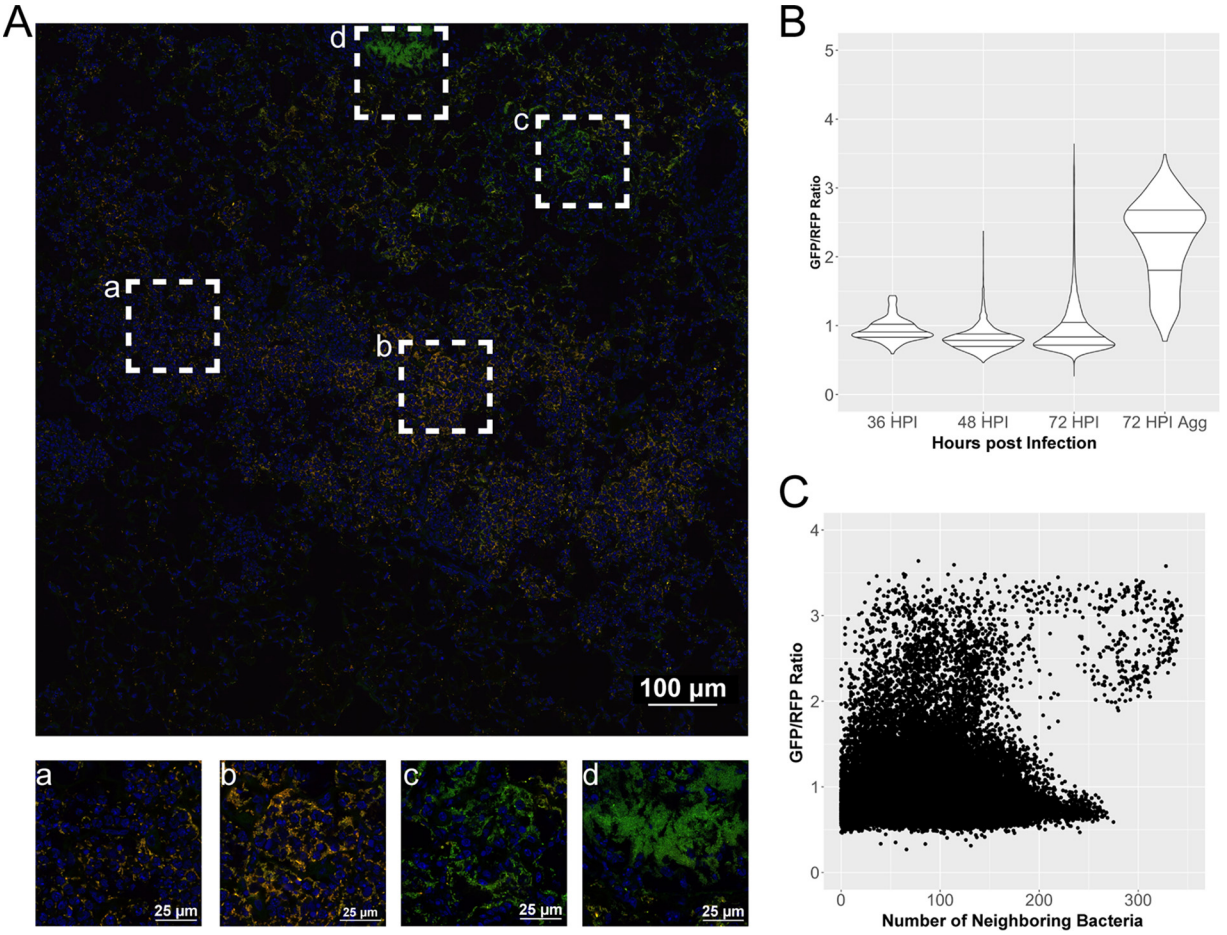

FIG 2 Expression of *crp* is increased in large aggregates or biofilm-like structures in the lungs. Cross sections of lungs from mice infected with strain CO92 carrying the P_{crp}-GFP reporter (green) and pGEN-RFP plasmid (red) were stained with DAPI (blue) and imaged by confocal microscopy. (A) Large image generated with the tile feature in NIS Elements acquisition software to cover *Y. pestis*-containing lesions within the lung space. Magnified images of boxed areas (a to d) highlight heterogeneity in expression patterns of *crp* within a single lesion. (B) Violin plots displaying the relative expression of *crp* as a ratio of GFP to RFP, quantified in individual cells combined from the lung lesions of at least three mice at each time point, across two independent infection experiments at 36, 48, and 72 hpi. Horizontal lines within the violins represent the 25th percentile, median, and 75th percentile. Aggregates were also imaged and analyzed separately. (C) Expression of *crp* in individual cells as a function of neighboring bacterial cell density from all images and time points postinfection.

of GFP to RFP in *Y. pestis* were observed when *gfp* was expressed from the *tetO* promoter (Fig. S1B and C).

In contrast, activity at the *crp* promoter was both spatially and temporally distinct (Fig. 2). While the mean GFP/RFP ratio at 72 hpi was not significantly higher than at 36 and 48 hpi, the population was skewed to higher levels of *crp* expression in a nonnormally distributed pattern (Fig. 2B). Observations of lung sections revealed bacteria within large aggregates of hundreds to thousands of bacterial cells with significantly higher *crp* expression levels, as determined by their GFP/RFP ratios. These large aggregates resembled biofilm-like structures with thousands of bacteria in close contact. When bacteria in biofilms were separated from the analysis, their mean GFP/RFP ratio was 2 to 3 times higher than that of the population as a whole (Fig. 2B). The number of cells in biofilms is underrepresented in this analysis as the algorithm detecting bacteria cannot always separate bacteria in contact with one another but, rather, records them as a single bacterium. There was no loss in RFP intensity alone between bacteria within the population as a whole and bacteria within biofilms, but the recorded GFP intensity alone was 2 to 3 times higher in bacteria in biofilms than in the rest of the population (Fig. S2A and B). This indicates that the differences observed in the GFP/RFP ratio are due to changes in regulation at the *crp* promoter and not due to

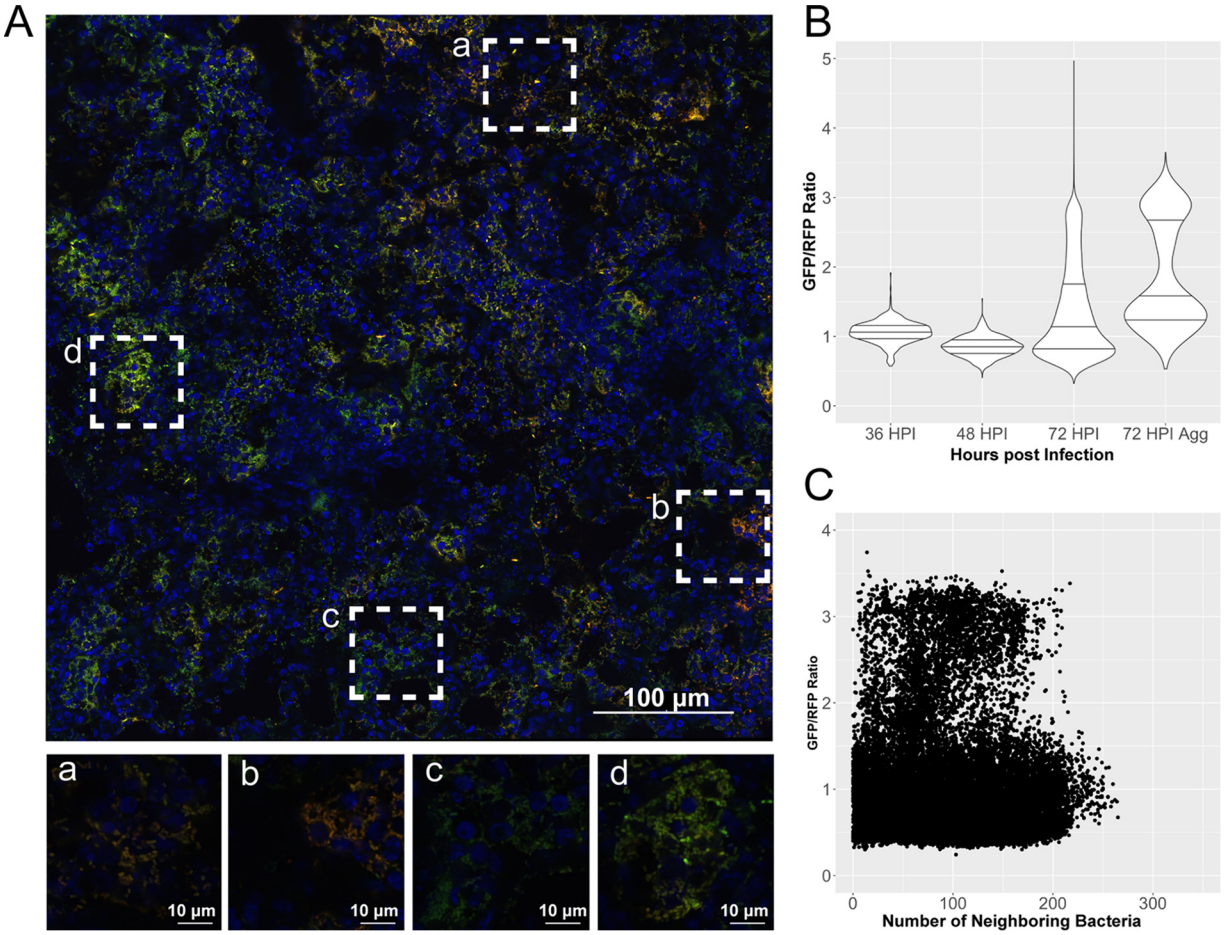

FIG 3 Expression of *pla* increases during progression of pneumonia independent of presence in a biofilm. Cross sections of lungs from mice infected with strain CO92 carrying the P_{pla}-GFP reporter (green) and pGEN-RFP plasmid (red) were stained with DAPI (blue) and imaged by confocal microscopy. (A) The large image was generated in NIS Elements similarly to infections with the P_{crp}-GFP strain. Magnified images of boxed areas (a to d) highlight the heterogeneity in expression patterns of *pla* within the larger lesion. (B) Violin plots displaying the relative expression of *pla* as a ratio of GFP to RFP, quantified in individual cells combined from the lung lesions of at least three mice at each time point, across two independent infection experiments at 36, 48, and 72 hpi. Horizontal lines within the violins represent the 25th percentile, median, and 75th percentile. Aggregates were also imaged and analyzed separately. (C) Expression of *pla* in individual cells as a function of neighboring bacterial cell density.

loss of the RFP plasmid or to artifacts introduced in acquisition or processing of the images.

In order to analyze expression of *crp* in higher-density aggregates in an unbiased fashion, relative expression based on the GFP/RFP ratio was plotted against the density of neighboring bacteria (Fig. 2C). The density of neighboring bacteria was determined by calculating the distances between all bacteria using their relative coordinate locations within a given image and reporting the number of neighboring bacterial cells within 30 μm. A comparison of all cells in all images indicated that there was significant heterogeneity in expression in lower-density bacteria ($<$150 neighboring cells), while higher-density cells ($>$175 neighboring cells) showed higher expression of *crp*. These observations of lung cross sections support the notion that expression of *crp* is increased within aggregates of bacteria within the lungs.

Expression of *pla* increases during progression of pneumonic plague. The virulence gene *pla* is known to be controlled by Crp (14). Expression of *pla* is repressed at the early stages of lung infection before rising more than 10-fold during the terminal stages of infection (13). To determine whether expression of *pla* displayed a spatially regulated pattern similar to that of *crp*, mice were intranasally infected with a strain harboring the P_{pla}-GFP fusion (Fig. 3A). Expression of *pla* was slightly reduced at 48 hpi

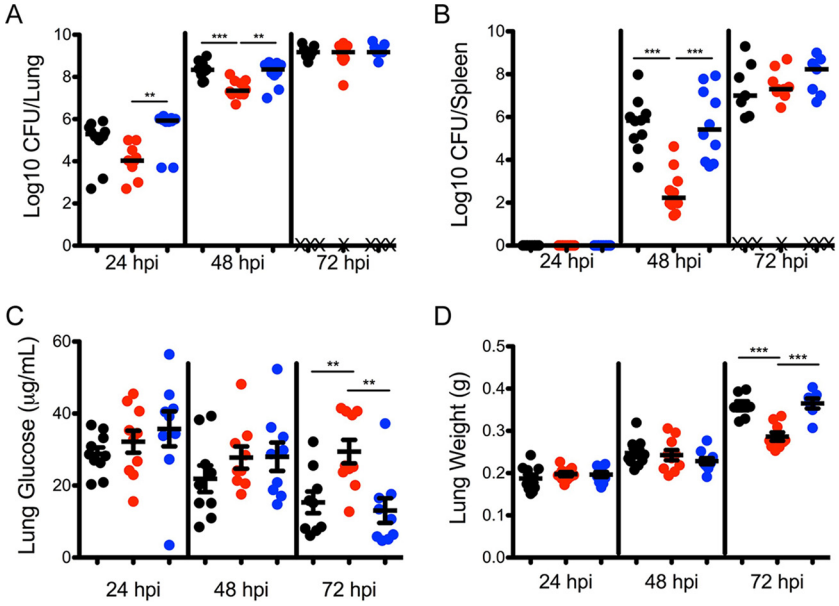

FIG 4 Deletion of *ptsG* from *Y. pestis* prevents depletion of glucose during infection. (A and B) Bacterial burden in the lungs (A) and spleens (B) of mice infected at 24, 48, and 72 hpi as follows: black, *Y. pestis*; red, *Y. pestis* Δ*ptsG*; blue, *Y. pestis* Δ*ptsG ptsG*. X, mouse succumbed to infection. (C) Concentration of glucose measured in BALF recovered from mice infected with *Y. pestis*, *Y. pestis* Δ*ptsG*, and *Y. pestis* Δ*ptsG ptsG*. (D) Wet lung weight of the lungs from mice infected as described for panel A. Data are combined from two independent infection experiments with five mice at each time point. Horizontal bars (A and B), medians; error bars (C and D), means and standard errors of the means. **, $P < 0.01$; ***, $P < 0.001$ (one-way ANOVA with Bonferroni multiple comparisons).

compared to the level at 36 hpi (Fig. 3B). At 72 hpi, however, there was a robust increase in global expression of *pla* within and around lesions in single and biofilm-assembled bacteria. In contrast to observations with the P_{crp}-GFP reporter, there was no correlation between presence within an aggregate and increased expression (Fig. 3B). Some aggregates observed did have high expression of *pla*, but there was no significant dependence on bacterial cell density, based on observations of all cells compared across all images, as regions with lower numbers of neighboring bacteria also showed high *pla* expression (Fig. 3C). Despite this, overall increased activity at the *pla* promoter at 72 hpi is consistent with increased *pla* transcript levels (13).

PtsG is required for glucose depletion in the lungs. To determine whether *Y. pestis* is responsible for consuming glucose in the lungs and whether glucose represses expression of *crp* and *pla*, a strain of *Y. pestis* lacking the EIIBC subunit of the glucose-specific phosphotransferase system (*Y. pestis* Δ*ptsG*) was made. Intranasal infection with *Y. pestis*, *Y. pestis* Δ*ptsG*, and *Y. pestis* Δ*ptsG* with *ptsG* reintroduced at the Tn*7* site (*Y. pestis* Δ*ptsG ptsG*) revealed that the *Y. pestis* Δ*ptsG* strain did not grow as well in the lungs as the parental and complemented strains at 24 and 48 hpi (Fig. 4A). These data indicate that PtsG is important for early colonization of the lungs. Across two independent experiments, mice infected with *Y. pestis* Δ*ptsG* did not develop symptoms as early as mice infected with strains containing *ptsG*, and more mice survived until 72 hpi despite having similar bacterial burdens. In addition, in mice infected with *Y. pestis* Δ*ptsG*, the average weight of the lungs harvested, an indirect measure of fluid accumulation in the lungs or edema, was on average 100 mg less than that in mice infected with the parental and complemented strains (Fig. 4D). In addition, *Y. pestis* Δ*ptsG* did not disseminate from the lungs to the spleen as well as the parental or complemented strain at 48 hpi (Fig. 4B). However, by 72 hpi, mice infected with *Y. pestis* Δ*ptsG* had bacterial burdens in the lungs and spleen indistinguishable from those of animals infected with the parental and complemented strains.

The concentration of glucose in the BALF from *Y. pestis* and *Y. pestis* Δ*ptsG ptsG* decreased as the pneumonia progressed to 72 hpi (Fig. 4C). In contrast, infection with

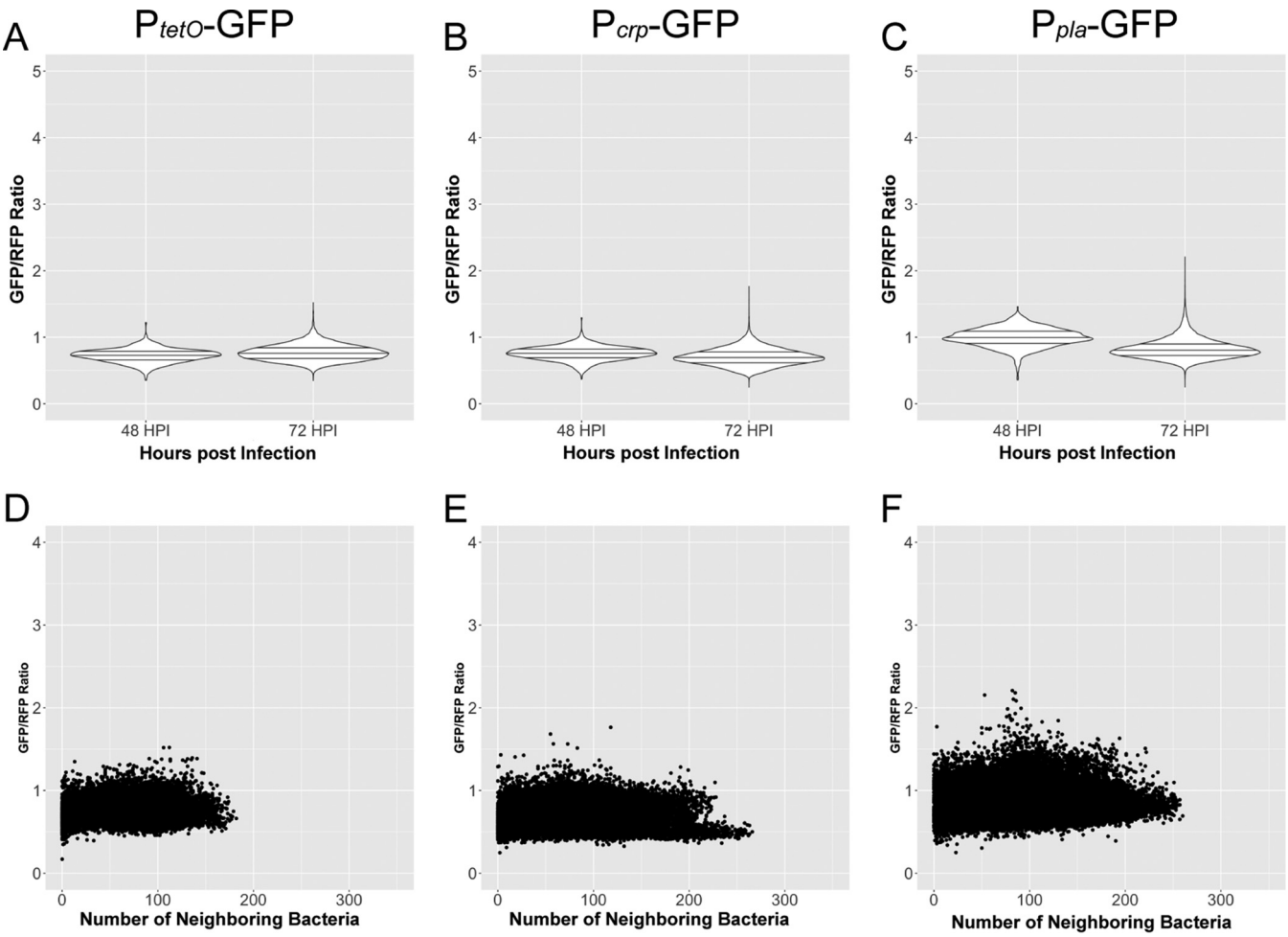

FIG 5 Expression levels of *crp* and *pla* do not increase during *Y. pestis* Δ*ptsG* infection. Cross sections of lungs from mice infected with *Y. pestis* Δ*ptsG* carrying the pGEN-RFP and either the P_{tetO}-GFP, P_{crp}-GFP, or P_{pla}-GFP reporter construct were analyzed identically to those from the wild-type-infected counterparts. (A to C) Violin plots of relative gene expression levels in individual cells combined from the lung lesions of at least three mice at each time point, across two independent infection experiments measured at 48 and 72 hpi for *Y. pestis* Δ*ptsG* expressing either the P_{tetO}-GFP, P_{crp}-GFP, or P_{pla}-GFP reporter construct, as indicated. Horizontal lines within the violins represent the 25th percentile, median, and 75th percentile. (D to F) Relative expression as a function of cell density for infection with *Y. pestis* Δ*ptsG* carrying the P_{tetO}-GFP, P_{crp}-GFP, or P_{pla}-GFP reporter construct. Individual points represent individual cells analyzed from infections at 48 and 72 hpi.

Y. pestis Δ*ptsG* did not result in a reduction in the concentration of glucose in the lungs, even in animals with identical CFU counts in the lungs at 72 hpi. These data suggest that *Y. pestis* is responsible for depletion of glucose, likely by increasing the import of glucose dependent upon PtsG.

Expression of *crp* and *pla* does not increase when glucose is present in the lungs. The *tetO*, *crp*, and *pla* reporter fusions were integrated into *Y. pestis* Δ*ptsG* carrying the pGEN-RFP plasmid in order to determine whether the difference in glucose concentrations within the lungs of *Y. pestis* Δ*ptsG*-infected mice affected expression of *crp* or *pla*. Bacteria could not be reliably detected by microscopy at 36 hpi due to the reduced bacterial burden of the *Y. pestis* Δ*ptsG* strain at this time point (Fig. 4A). Bacteria could be imaged in lung cross sections at 48 and 72 hpi using images comparable to those obtained from infections with the wild-type strain. Similar to infections with the parent strain, there was no spatiotemporal regulation of the constitutive *tetO* promoter or dependence on the density of the bacterial cells (Fig. 5A and D). But, in contrast to what was observed with the parental strain, the distribution of expression of *crp* as measured by the P_{crp}-GFP fusion was not skewed to higher levels at 72 hpi, and expression was not increased in aggregates or biofilms of high cellular densities within the lungs (Fig. 5B and E). Expression of *pla* was also significantly

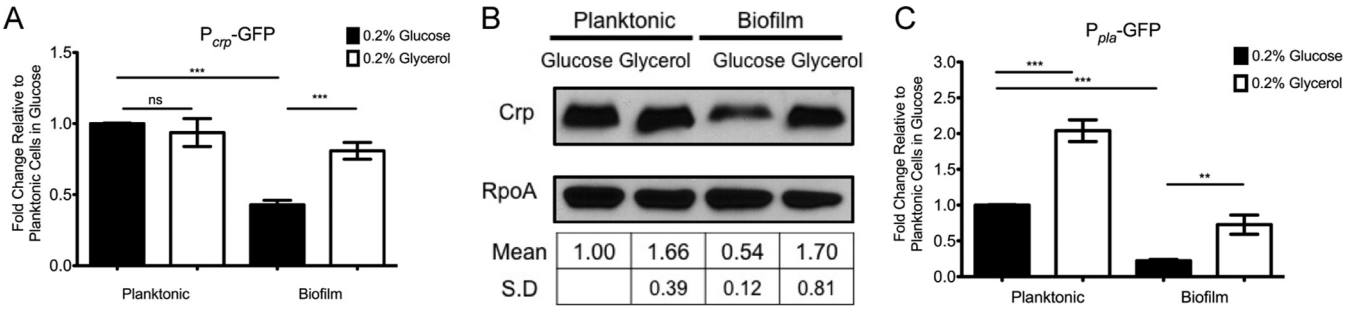

FIG 6 Expression of *crp* is repressed by glucose in biofilms *in vitro*. (A) *Y. pestis* Lcr$^-$ with the P_{crp}-GFP reporter was grown in 10 ml of TMH medium supplemented with 0.2% glucose or 0.2% glycerol. Planktonic bacteria growing within the medium were separated from bacteria in the biofilm formed at the air-liquid interface on the flask, and fluorescence intensity was measured and standardized to that of planktonic cells in 0.2% glucose. (B) Representative blot from whole-cell lysates generated from *Y. pestis* Lcr$^-$ grown as described for panel A and immunoblotted for Crp protein. RpoA was used as a loading control, and blots were quantified in Fiji and standardized to planktonic cells in 0.2% glucose. (C) *Y. pestis* Lcr$^-$ carrying the P_{pla}-GFP reporter was grown as described for panel A. Fluorescence intensity from the reporter was measured and standardized to that of planktonic cells in 0.2% glucose. Data are representative of three independent experiments. Error bars represent the means and standard errors of the means. **, $P < 0.01$; ***, $P < 0.001$; ns, not significant (one-way ANOVA with Bonferroni multiple-comparison test).

reduced in measurements of *Y. pestis* Δ*ptsG* containing the P_{pla}-GFP fusion, which lacked the robust increase measured in the wild-type strain (Fig. 5C and F). In fact, measurements of both *crp* and *pla* reporter strains lacking *ptsG* resembled measurements taken of the *tetO* reporter, which exhibited no spatial or temporal expression. No difference in expression levels of *crp* or *pla* was observed between the wild-type and Δ*ptsG* mutants *in vitro* (Fig. S3), suggesting not only that PtsG is required to consume glucose from the lungs during pneumonia but also that this absence of glucose is required for activating expression of *crp* in biofilms and activating expression of *pla* through catabolite repression.

Glucose represses expression of *crp* and *pla* in biofilms grown *in vitro*. To model the effect of glucose on expression of *crp* in biofilms, fluorescence was measured in *Y. pestis* containing the P_{crp}-GFP fusion in planktonic cells and cells within biofilms. Consistent with the *in vivo* findings, the presence or absence of glucose had no effect on GFP fluorescence as measured by the P_{crp}-GFP reporter in the planktonic state (Fig. 6A). However, *Y. pestis* growing within a biofilm in the presence of glucose was repressed 2-fold compared to growth in a biofilm in the presence of glycerol. Similar trends in expression of *crp* were observed in the absence of membrane-bound adenylate cyclase (Fig. S4A), indicating that the mechanism of activation of *crp* expression in the absence of glucose is surprisingly not dependent on adenylate cyclase activity. A similar trend was observed when whole-cell lysates (WCLs) from *Y. pestis* grown under the same conditions were immunoblotted for Crp protein (Fig. 6B). As with growth with supplemental glycerol, Crp protein levels were not repressed in biofilms grown in the presence of 0.2% galactose or 0.2% sucrose (Fig. S4B). Expression of *pla* was repressed by glucose in both the planktonic and biofilm states as measured in strains harboring the P_{pla}-GFP reporter (Fig. 6C).

Overall, these data are consistent with control of *pla* expression by changes in cAMP and are also consistent with changes in Crp levels due to depletion of glucose in the biofilm state. Together, these *in vitro* findings are consistent with observations in the lungs that expression of *crp* is stimulated by growth in biofilms, while expression of *pla* is activated by catabolite repression.

Increased expression of *crp* in biofilms requires the *crp* 5′ UTR. Previous work found that the sRNA chaperone Hfq acts at the *crp* 5′ UTR to promote translation of *crp* (13). To determine whether the *crp* 5′ UTR is necessary for regulation of *crp* in biofilms, a GFP fusion containing the *crp* promoter with the *tetO* 5′ UTR replacing the *crp* 5′ UTR (P_{crp}-*tetO* 5′ UTR-GFP) was integrated into *Y. pestis*. Expression of this reporter was regulated neither by carbon source nor by growth in the planktonic or biofilm state (Fig. 7A). Furthermore, infection with fully virulent *Y. pestis* with this fusion did not result in increased expression at 72 hpi or within high-density aggregates in the lungs

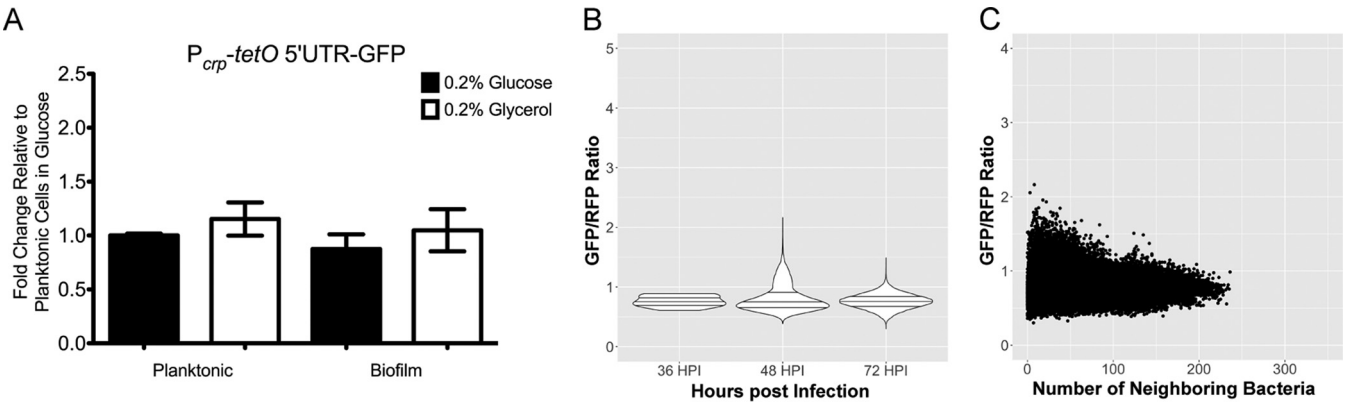

FIG 7 Increased expression of *crp* in biofilms requires the *crp* 5′ UTR. (A) *Y. pestis* with the P$_{crp}$-*tetO* 5′ UTR-GFP reporter was grown in TMH medium supplemented with 0.2% glucose or 0.2% glycerol overnight. Planktonic and biofilm cells were separated, and GFP intensity was standardized to that of planktonic cells grown in 0.2% glucose. (B) Cross sections from mice infected with *Y. pestis* CO92/pGEN-RFP containing the P$_{crp}$-*tetO* 5′ UTR-GFP reporter construct were imaged by confocal microscopy at 36, 48, and 72 hpi. Violin plots show the distribution of expression from single cells combined from at least three lung cross sections from the lung lesions of at least three mice at each time point, across two independent infection experiments. Horizontal lines within the violins represent the 25th percentile, median, and 75th percentile. (C) Relative expression as a function of density of neighboring *Y. pestis* cells measured from the P$_{crp}$-*tetO* 5′ UTR-GFP reporter construct.

of infected mice (Fig. 7B and C), suggesting that the mechanism regulating expression of *crp* in biofilms occurs at the posttranscriptional level.

DISCUSSION

Y. pestis requires the plasminogen activator protease in order to cause both bubonic and pneumonic forms of plague (7, 8). Thus, it was surprising to find that expression of *pla* is repressed early within the lungs, and its expression only increased during later stages of infection (13). The goal of this study was to determine if the changing sources of carbon during infection can impact control of this important virulence gene. Due to the complexity of the lung environment and potential for multiple stimuli involved in the control of gene expression, an approach using GFP reporter fusions combined with confocal microscopy was used to uncover spatial and temporal changes in gene expression. A similar approach was used for studying *Yersinia pseudotuberculosis* regulation of *hmp* and *yopE* genes in response to reactive nitrogen species production and proximity to host cells, highlighting the usefulness of such approaches for studying host-microbe interactions (27).

Previous work found that cAMP-Crp activates expression of *pla in vitro*, but it was unknown whether the carbon source would change during infection and whether this *in vitro* finding was relevant during pneumonic plague disease (13, 14). During lung infection, it was found that the concentration of glucose decreased more than 5-fold in the lavage fluid from mice infected with the wild-type strain of *Y. pestis* at 72 hpi (Fig. 1A). Most of the infected mice had lung glucose concentrations of less than 1 μg/ml (Fig. 1B). Levels of glucose are typically 10 to 20 times higher in the blood than in the lungs, and this difference is maintained by passive diffusion of glucose from the blood and active transport out of the alveolar space (28). Because mouse serum albumin was detected in the lungs at 48 hpi, glucose should be present in the lungs by diffusion from the vasculature and surrounding interstitium. These observations suggest that *Y. pestis* utilizes glucose at a significant rate as an energy source. Expression of genes for the tricarboxylic acid (TCA) cycle was repressed during pneumonia in mice and was not required for bubonic plague infection in rats (6, 29), indicating that generation of energy through glycolysis is important for *Y. pestis* infection. However, we cannot entirely exclude the possibility that near the end of infection, glucose levels are depleted from the lungs due to changes in the food consumption behavior or metabolism of infected mice although levels of glucose in the BALF of uninfected mice (31.8 $\pm$ 11.3 μg/ml, $n = 5$) and fasted mice (36.8 $\pm$ 8.9 μg/ml, $n = 5$) for 16 h (a time

comparable to when symptoms are apparent in mice and when mice succumb to infection) were not significantly different.

This dramatic drop in glucose would be expected to activate catabolite repression to facilitate consumption of alternative carbon sources as the infection progresses. Indeed, increased activity of the *crp* promoter in lungs was evident. Interestingly, this increase was mostly observed in large bacterial aggregates that resembled biofilms within the lungs of infected mice (Fig. 2A). While this difference was both visually observable and readily measurable, there were also many bacteria not present in biofilms with increased expression levels of *crp* or with significantly fewer neighboring cells (Fig. 2C), indicating that other stimuli can also contribute to activation of *crp* expression in the lungs, independent of biofilm formation.

The mechanism of increased activity at the *crp* promoter was modeled also *in vitro* using biofilms formed in flasks. Minimal medium, thoroughly modified Higuchi's (TMH) medium, was shown to promote robust biofilm formation at 37°C. While expression of *crp* in planktonic cells was not affected by carbon source, expression of *crp* was stimulated in bacteria growing in a biofilm with the alternative carbon source glycerol, galactose, or sucrose (see Fig. S4B in the supplemental material) but was reduced in biofilms growing in glucose. These data support observations of *Y. pestis* in the lung and suggest that, when glucose becomes limiting, *Y. pestis* may utilize other carbon sources through activation of catabolite repression, particularly in bacteria growing within biofilms. Surprisingly, the repression of *crp* by glucose occurs independently of the presence of adenylate cyclase (Fig. S4A). These observations suggest that the mechanism regulating expression of *crp* in *Y. pestis* is different from regulation of *crp* in *E. coli* (24, 30).

In addition, this study indicates that posttranscriptional regulation may impact the expression of *crp*. Expression of a GFP fusion containing the upstream promoter of *crp* with the *crp* 5′ UTR replaced with the *tetO* 5′ UTR (P_{crp}-*tetO* 5′ UTR-GFP) was not repressed in bacteria grown in biofilms, indicating the requirement of the *crp* 5′ UTR for glucose-mediated repression (Fig. 7A). This reporter was also not activated in large bacterial aggregates in the lungs of infected mice, suggesting that the *crp* 5′ UTR is also required for activation of the *crp* promoter during infection (Fig. 7B). Future research directions will include determining the mechanism operating at the *crp* 5′ UTR, including if sRNAs and Hfq promote Crp translation (13).

As a link to virulence, expression of the virulence factor *pla* was also monitored *in vivo*. There was temporal regulation of *pla* with more robust activity of the *pla* promoter at 72 hpi than at 36 and 48 hpi, an observation consistent with previous experiments measuring *pla* transcript levels during pneumonia (13). There were some cells that did not express *pla* as highly, and, in contrast to findings with the *crp* promoter, increased expression of *pla* in cells was independent of the number of neighboring cells (Fig. 3C). Further distinguishing *pla* and *crp* regulation, *in vitro* studies revealed that expression of *pla* requires adenylate cyclase for cAMP-Crp production and is elevated in both planktonic and biofilm states in the absence of glucose (14) (Fig. 6C). Given the significant global reduction of glucose measured in the lungs at 72 hpi (Fig. 1A), intracellular concentrations of cAMP would be higher during later infection than during earlier time points. While expression of *crp* was noticeably higher within biofilms in the lungs, many bacteria in lower cell densities had increased expression of *crp* that would also contribute to increased expression of *pla*. This heterogeneity in expression of *pla* could be explained due to spatial differences in the concentration of glucose such that different populations of *Y. pestis* consume glucose differentially, activating *pla* when glucose becomes depleted. In biofilms, the significant reduction in glucose would also stimulate production of additional Crp.

To determine whether PtsG contributed to expression of *crp* and *pla*, the same spatial and temporal expression analyses were performed with *Y. pestis* Δ*ptsG* strains harboring the P_{crp}-GFP and P_{pla}-GFP reporters. In contrast to infections with the parent strain, there were no spatial or temporal differences in the activity of *crp* or *pla* (Fig. 5B and C). This suggests that PtsG contributes to increased expression of *crp* and *pla*

during pneumonia. There was no difference in the production levels of Crp and Pla protein between wild-type and Δ*ptsG* mutant strains when they were grown *in vitro* (Fig. S3), indicating that the reduction in *crp* and *pla* expression levels *in vivo* is not due to direct effects of PtsG on either gene but, rather, to the necessity of PtsG to deplete glucose from the lung environment. Our attempts to restore glucose levels during late infection with exogenous glucose were met with technical issues in delivering glucose to the lungs in moribund mice. In the absence of PtsG, *Y. pestis* may use less efficient glucose transport systems, such as *manXYZ*, which is upregulated in *Y. pestis*-infected lungs and would still repress cAMP production in the presence of glucose (6, 31). These important findings with the *Y. pestis* Δ*ptsG* strain demonstrate the importance of glucose not only as a carbon source for *Y. pestis* to proliferate early in the lungs but also as a signal to activate expression of *crp* and *pla* when glucose becomes limiting.

Another important observation from mice infected with *Y. pestis* Δ*ptsG* was the lack of increased lung weight during the progression of disease. Infection with wild-type *Y. pestis* may limit the host's ability to clear fluid through glucose/Na^+ transporters by taking up glucose through PtsG, leading to a more severe pneumonia (28). Mice infected with *Y. pestis* Δ*ptsG* had increased survival at 72 hpi, exhibited less severe symptoms of disease, and had an average lung weight 100 mg less than that of mice infected with wild-type *Y. pestis*, suggesting that PtsG contributes to increased edema in the lungs and disease severity. Recently, tissue dual-transcriptome sequencing (RNA-seq) was applied to *Y. pseudotuberculosis*-infected mice and uncovered that *Y. pseudotuberculosis* increased expression of *ptsG* and other sugar transporter genes during infection (32). In addition, tissue dissected from the infected mice showed reduced expression of host glucose-specific transporters (33). In this context, the inability of the host to transport carbohydrates out of the lumen contributes to increased diarrheal disease. By analogy, the inability to transport glucose would result in increased edema. We also cannot exclude alternative explanations such as the influx of neutrophils, and the subsequent inflammatory responses could deplete glucose in the lungs and could be different between wild-type- and Δ*ptsG*-infected mice. Neutrophils have also been shown to regulate their gene expression spatially within the lungs (34), and we cannot fully exclude their contributions to expression of *crp* and *pla* during infection. However, we did observe identical bacterial burdens between wild-type- and Δ*ptsG* mutant-infected mice at 72 hpi and observed neutrophils (by nucleus shape stained with 4′,6′-diamidino-2-phenylindole [DAPI]) recruited to the lungs of mice infected with both strains, suggesting that bacteria are at least a major source of glucose depletion.

Several studies have utilized diabetic mouse models to demonstrate the impact that excess glucose has on increasing bacterial proliferation within the lungs (35, 36). Levels of glucose in the lungs are maintained lower in order to prevent colonization of pathogens (37). However, colonization of the lungs still occurs, and, as shown here, pathogens such as *Y. pestis* sense lowered glucose concentration as a signal for activating virulence gene expression. This may not be a common tactic of all lung pathogens. The concentration of glucose remained constant during infection with *Mycobacterium tuberculosis* and *Pseudomonas aeruginosa* during disease progression (35, 38). *M. tuberculosis* and *P. aeruginosa* lack glucose-specific PtsG homologs and instead use other pathways or metabolites, such as lipolysis of phosphatidylcholine or catabolism of succinate, to proliferate within the lungs. Understanding how bacteria utilize and regulate virulence gene expression in response to different carbon sources or metabolites during infection could open new therapeutic opportunities through manipulation of the pathogen's environment.

Overall, while catabolite repression has been studied extensively *in vitro*, this work is the first to describe how catabolite repression and the phosphotransferase system act to regulate virulence gene expression in the context of infection in response to changing carbon source availability. Furthermore, the ability of *Y. pestis* to acquire glucose from the lungs is necessary for efficient colonization of the lungs and may impact the host's ability to clear fluid from the lungs as pneumonia progresses. Given

that cAMP-Crp regulates expression of many pertinent metabolic and virulence genes across many species of pathogens, cAMP-Crp in general may serve as a critical sensor of nutrient availability, integrating changes in the concentration of glucose and PTS substrates into changes in gene expression.

MATERIALS AND METHODS

Bacterial strains, reagents, and culture conditions. Bacterial strains used in this study are listed in Table S1 in the supplemental material, plasmids and their descriptions are give in Table S2, and oligonucleotides are listed in Table S3. Work with fully virulent select agent strains of *Y. pestis* CO92 and subsequent animal infections were performed in CDC-approved biosafety level 3 (BSL-3) and animal BSL-3 facilities at Northwestern University. The pCD1, pMT1, pPCP1, and *pgm* loci were confirmed upon new strain generation by PCR. Routine passage and mutagenesis of *Y. pestis* was performed on brain heart infusion (BHI) agar (Difco) at 26°C. Overnight cultures at 26°C were started in 2 ml of either BHI broth or in defined TMH broth (39), supplemented with 0.2% glucose, glycerol, galactose, or sucrose as indicated in the figures, and back diluted in fresh medium at an optical density at 620 nm (OD_{620}) of 0.1 in 10 ml of broth in a 125-ml Erlenmeyer flask incubated with shaking at 250 rpm at 37°C. Ampicillin (100 μg/ml) and kanamycin (50 μg/ml) were added when necessary. $CaCl_2$ (2.5 mM) was added to medium for growth of fully virulent ($pCD1^+$) strains at 37°C for animal infections.

Reporter strains measuring GFP fluorescence from *crp*, *pla*, or *tetO* promoters were integrated into the Tn*7* site as described previously. The P_{tetO}-GFP construct was generated by PCR amplifying the *tetO* promoter from pWL213 and the coding sequence (CDS) of *gfp* from pROBE-GFP. The two fragments were joined by spliced overlap extension PCR (SOE-PCR), and the P_{tetO}-GFP fragment was cloned into the pUC18-R6k-miniTn7t vector lacking the *tet* repressor. These constructs were integrated into the Tn*7* site of fully virulent *Y. pestis* CO92 with the pTNS2 helper plasmid (40). The pGEN-RFP plasmid was electroporated into these strains and selected for on ampicillin and virulence loci confirmed by PCR (41). Tn*7* integration and presence of the pGEN-RFP plasmid did not affect virulence, and the RFP plasmid was maintained throughout infection. The Δ*ptsG* mutant was generated by lambda red recombination by amplification of ~500 bp upstream and downstream of *ptsG* with primer pairs P1993/P1994 and P1995/P1996, respectively, and in-frame deletions with leftover scar sequence were generated as previously described (42). Complementation of the *ptsG* mutant was accomplished by amplifying 500 bp upstream and downstream of the *ptsG* gene with primers P1997 and P1998 and cloned into the multiple cloning site of pUC18-R6K-miniTn7t. Complementation was completed by Tn*7*, and integration of the plasmid into the Δ*ptsG* mutant strain was confirmed by PCR.

Animal experiments. All animal experiments were performed in compliance with the Northwestern University IACUC policies. Six- to 8-week-old C57BL/6 mice from Jackson Laboratory (Bar Harbor, ME) were used for all animal infections and housed within the animal BSL-3 facility at Northwestern University for duration of infection experiments. Mice were given mouse chow to eat *ab libitum*. Chow was wetted with water and placed in the cage near mice to encourage feeding when mice exhibited symptoms of pneumonia. Inocula for infections were prepared as described previously (12), and infections with strains harboring the pGEN-RFP plasmid were supplied with ampicillin during inoculum preparation. For infections, mice were anesthetized with a mixture of ketamine-xylazine and euthanized by administration of a lethal dose of pentobarbital at time points for data collection indicated in the figures. CFU count determinations were performed by plating whole lungs homogenized in 500 μl of phosphate-buffered saline (PBS). BALF was recovered by tracheal cannulation and inflation of the lungs once with 1 ml of PBS. The recovered fluid (~700 μl) was centrifuged at 4°C at 14,800 $\times$ *g* for 2 min to pellet cells within the lavage fluid, and cells and fluid were stored at −80°C for future analyses. The supernatant fluid was filter-sterilized through 0.22-μm-pore-size filter to obtain cell-free lavage fluid which was plated for growth on BHI agar before use in downstream applications. Blood was recovered from infected animals by cardiac puncture. Briefly, a Luer Lock 31-gauge, 0.5-in. needle was inserted into the left ventricle of mice immediately following euthanasia, and ~100 μl of whole blood was recovered and stored in 10% heparin. Serum was obtained by centrifuging whole blood at 14,800 $\times$ *g* for 5 min at 4°C, and the supernatant was collected and stored at −80°C.

Fluorescence microscopy of lung cross sections. Infected mouse lungs were prepared for cross sectioning as follows. At the time points postinfection indicated in the figures, mice were euthanized, and the lungs were slowly inflated with 1 ml of 4% paraformaldehyde (PFA) in PBS (pH 7.2) by tracheal cannulation and tied off with suture string. Lungs were excised and stored overnight in 50-ml conical tubes containing 30 ml of 4% PFA. PFA (4%) was exchanged for 15% sucrose in PBS (pH 7.2) the next day for 8 h before exchange into 30% sucrose overnight. Whole lungs were frozen embedded in 22-oxacalcitriol (OCT) medium in a dry ice-ethanol bath and stored for at least 48 h at −80°C at the Northwestern University Mouse Histology and Phenotyping Laboratory (MHPL). Ten-micrometer cross sections were cut with a cryostat and adhered to glass slides overnight and then stained with DAPI (4′, 6-diamidino-2-phenylindole). Slides were imaged on a Nikon A1R confocal microscope with GaAsP detectors. Three-color images were obtained by sequential imaging at wavelengths of 405 nm, 488 nm, and 561 nm for obtaining signals from DAPI staining, from GFP from respective reporter constructs, and from RFP from the constitutive *rfp*-expressing plasmid, pGEN-RFP.

Large images of lung sections were generated with the tile feature of NIS Elements imaging software with no overlap. Raw.nd2 files were exported to Fiji software for data analysis (43). GFP/RFP ratios were calculated from individual cells through an in-house-derived macro for identifying and recording signal intensity in each channel of individual bacteria. Briefly, bacteria were identified by RFP intensity with a

minimum average intensity of >500 to limit detection to only RFP-positive bacteria. Particle areas were copied to the GFP channel where intensity from the reporter construct was determined. The GFP and RFP intensities from each cell were measured, and the ratio GFP/RFP was calculated in Microsoft Excel. Images of aggregates were taken from the same cross sections and imaged and analyzed separately. Violin plots were generated in R (version 3.3.2) using the tidyverse package (version 1.1.1). The number of nearby neighboring cells was calculated by exporting the relative *xy* coordinates of the center of identified bacteria in entire lung sections in Fiji and calculating the distance matrix between all coordinates in R with the fields (version 9.0) and matrix (version 1.2-11) packages. The number of bacteria with a distance of <30 μm was returned and correlated with the GFP/RFP ratio using the tidyverse package in R.

GFP reporter assays. GFP reporter assays were performed as described previously (13). Cultures were grown for 6 h at 26°C in TMH medium supplemented with either 0.2% glucose or glycerol, back-diluted into fresh medium at an OD_{620} of 0.1 in 10 ml, and incubated in an 125-ml Erlenmeyer flask with shaking at 250 rpm. Planktonic and biofilm cells were separated by careful removal of the medium with a serological pipette. Biofilm cells at the air-liquid interface were resuspended in 1 to 5 ml of PBS by scraping and vortexing vigorously. Planktonic and biofilm suspensions were normalized to an OD_{620} of 0.25 in PBS and transferred in 200 μl to a 96-well plate in duplicate, and fluorescence was read on a Tecan Safire II plate reader. Fluorescence was standardized to the OD_{620} and normalized to reporter strains containing the GFP coding sequence alone without a promoter.

Measurement of glucose concentration. Glucose concentration in serum or BALF was measured with a Glucose GO kit (Sigma) scaled down accordingly. Forty microliters of BALF was incubated with 80 μl of assay reagent in a 96-well plate for 30 min at 37°C and inactivated by addition of 80 μl of 6 M sulfuric acid. Absorbance was read on a Molecular Devices SpectraMax M5 microplate reader at 540 nm. Serum glucose levels were measured by diluting serum 1:20 in distilled H_2O (dH_2O) to a volume of 100 μl with 200 μl of assay reagent for 30 min at 37°C and inactivated with 200 μl of 6 M sulfuric acid. Absorbance at 540 nm was read in 1-cm cuvettes with a Biomate 3 spectrophotometer (Fisher Scientific).

Measurement of plasmin activity. Plasmin activity was determined as described previously (10). BALF (100 μl) was incubated in the presence of 50 μM D-AFK-ANSNH-iC4H9-2Hbr fluorogenic substrate (SN5; Hematologic Technologies), and fluorescence was recorded over time at 460 nm in 96-well plates with a Molecular Devices SpectraMax M5 fluorescence microplate reader.

Measurement of mouse serum albumin levels. Mouse serum albumin was measured with a mouse serum albumin enzyme-linked immunosorbent assay (ELISA) from Immunology Consultants Laboratory, Inc. (12). BALF was diluted 5,000- to 50,000-fold in dilution buffer according to the manufacturer's instructions. Concentration of albumin was calculated by generating a standard curve from the provided standards.

Immunoblotting. Cultures of *Y. pestis* were grown overnight in 2 ml of BHI or defined TMH broth at 26°C, back diluted in 10 ml of fresh BHI or TMH broth (with 0.2% glucose, glycerol, galactose, or sucrose), and incubated at 37°C with shaking for 6 h. Whole-cell lysates (WCL) were generated by centrifuging 1 OD_{620} equivalent of cells at 14,800 $\times$ *g* for 2 min and resuspended in 100 μl of PBS. For comparisons between planktonic and biofilm cells, cells were grown for 16 h at 37°C, and the planktonic and biofilms were separated as described for measuring fluorescence from reporter strains. One hundred microliters of loading buffer (4% SDS, 20% glycerol, 120 mM Tris-Cl [pH 6.8], bromophenol blue 0.02%) was added, and cells were boiled for 10 min at 100°C. Ten microliters of WCL was loaded onto SDS-PAGE gels and transferred to nitrocellulose membrane. Antibodies were diluted 1:100,000 for RpoA (Melanie Marketon, Indiana University), 1:2,000 for Crp (clone 1D8D9; BioLegend), and 1:100 for Pla (44) and probed with horseradish peroxidase (HRP)-conjugated secondary antibodies at 1:2,000 (Sigma) and developed on X-ray film. Membranes were stripped (in 25 ml of 6.25 mM Tris HCl, pH 6.8, 2% SDS, 0.004% β-mercaptoethanol) at 55°C and reprobed with different primary antibodies as necessary. Band intensities were calculated in Fiji and standardized to the level of RpoA.

Statistical analyses. Student's *t* tests and one-way analysis of variance (ANOVA) with Bonferroni multiple-comparison tests were performed in GraphPad Prism, version 5.0, using a *P* value of <0.05 as a cutoff for significance.

SUPPLEMENTAL MATERIAL

Supplemental material for this article may be found at https://doi.org/10.1128/JB.00737-17.

SUPPLEMENTAL FILE 1, PDF file, 1.1 MB.

ACKNOWLEDGMENTS

We thank members of the Wyndham W. Lathem laboratory and Karla J. F. Satchell for their helpful support and discussions regarding this work. We thank Bill Goldman for the pGEN-RFP plasmid and Melanie Marketon for the RpoA antibody used throughout this work.

Histology services were provided by the Northwestern University Mouse Histology and Phenotyping Laboratory supported by NCI P30-CA060553, awarded to the Robert H. Lurie Comprehensive Cancer Center. Imaging work was performed at the Northwestern University Center for Advanced Microscopy generously supported by NCICCSG

P30-CA060553, awarded to the Robert H. Lurie Comprehensive Cancer Center. Use of the Tecan Safire II plate reader provided by the Northwestern University Structural Biology Facility was supported by NCICSG P30-CA60553. This work was supported by grant R21AI111018 from the National Institute of Allergy and Infectious Diseases.

REFERENCES

1. Perry RD, Fetherston JD. 1997. Yersinia pestis—etiologic agent of plague. Clin Microbiol Rev 10:35–66.
2. Pechous RD, Sivaraman V, Price PA, Stasulli NM, Goldman WE. 2013. Early host cell targets of Yersinia pestis during primary pneumonic plague. PLoS Pathog 9:e1003679. https://doi.org/10.1371/journal.ppat.1003679.
3. Pechous RD, Sivaraman V, Stasulli NM, Goldman WE. 2016. Pneumonic plague: the darker side of Yersinia pestis. Trends Microbiol 24:190–197. https://doi.org/10.1016/j.tim.2015.11.008.
4. Chauvaux S, Rosso ML, Frangeul L, Lacroix C, Labarre L, Schiavo A, Marceau M, Dillies MA, Foulon J, Coppee JY, Medigue C, Simonet M, Carniel E. 2007. Transcriptome analysis of Yersinia pestis in human plasma: an approach for discovering bacterial genes involved in septicaemic plague. Microbiology 153:3112–3124. https://doi.org/10.1099/mic.0.2007/006213-0.
5. Vadyvaloo V, Jarrett C, Sturdevant DE, Sebbane F, Hinnebusch BJ. 2010. Transit through the flea vector induces a pretransmission innate immunity resistance phenotype in Yersinia pestis. PLoS Pathog 6:e1000783. https://doi.org/10.1371/journal.ppat.1000783.
6. Lathem WW, Crosby SD, Miller VL, Goldman WE. 2005. Progression of primary pneumonic plague: a mouse model of infection, pathology, and bacterial transcriptional activity. Proc Natl Acad Sci U S A 102:17786–17791. https://doi.org/10.1073/pnas.0506840102.
7. Lathem WW, Price PA, Miller VL, Goldman WE. 2007. A plasminogen-activating protease specifically controls the development of primary pneumonic plague. Science 315:509–513. https://doi.org/10.1126/science.1137195.
8. Sodeinde OA, Subrahmanyam YV, Stark K, Quan T, Bao Y, Goguen JD. 1992. A surface protease and the invasive character of plague. Science 258:1004–1007. https://doi.org/10.1126/science.1439793.
9. Caulfield AJ, Walker ME, Gielda LM, Lathem WW. 2014. The Pla protease of Yersinia pestis degrades Fas ligand to manipulate host cell death and inflammation. Cell Host Microbe 15:424–434. https://doi.org/10.1016/j.chom.2014.03.005.
10. Eddy JL, Schroeder JA, Zimbler DL, Bellows LE, Lathem WW. 2015. Impact of the Pla protease substrate alpha2-antiplasmin on the progression of primary pneumonic plague. Infect Immun 83:4837–4847. https://doi.org/10.1128/IAI.01086-15.
11. Eddy JL, Schroeder JA, Zimbler DL, Caulfield AJ, Lathem WW. 2016. Proteolysis of plasminogen activator inhibitor-1 by Yersinia pestis remodulates the host environment to promote virulence. J Thromb Haemost 14:1833–1843. https://doi.org/10.1111/jth.13408.
12. Zimbler DL, Schroeder JA, Eddy JL, Lathem WW. 2015. Early emergence of Yersinia pestis as a severe respiratory pathogen. Nat Commun 6:7487. https://doi.org/10.1038/ncomms8487.
13. Lathem WW, Schroeder JA, Bellows LE, Ritzert JT, Koo JT, Price PA, Caulfield AJ, Goldman WE. 2014. Posttranscriptional regulation of the Yersinia pestis cyclic AMP receptor protein Crp and impact on virulence. mBio 5:e01038-13. https://doi.org/10.1128/mBio.01038-13.
14. Kim TJ, Chauhan S, Motin VL, Goh EB, Igo MM, Young GM. 2007. Direct transcriptional control of the plasminogen activator gene of Yersinia pestis by the cyclic AMP receptor protein. J Bacteriol 189:8890–8900. https://doi.org/10.1128/JB.00972-07.
15. Nuss AM, Heroven AK, Waldmann B, Reinkensmeier J, Jarek M, Beckstette M, Dersch P. 2015. Transcriptomic profiling of Yersinia pseudotuberculosis reveals reprogramming of the Crp regulon by temperature and uncovers Crp as a master regulator of small RNAs. PLoS Genet 11:e1005087. https://doi.org/10.1371/journal.pgen.1005087.
16. Deutscher J, Ake FM, Derkaoui M, Zebre AC, Cao TN, Bouraoui H, Kentache T, Mokhtari A, Milohanic E, Joyet P. 2014. The bacterial phosphoenolpyruvate:carbohydrate phosphotransferase system: regulation by protein phosphorylation and phosphorylation-dependent protein-protein interactions. Microbiol Mol Biol Rev 78:231–256. https://doi.org/10.1128/MMBR.00001-14.
17. Escalante A, Salinas Cervantes A, Gosset G, Bolivar F. 2012. Current knowledge of the Escherichia coli phosphoenolpyruvate-carbohydrate phosphotransferase system: peculiarities of regulation and impact on growth and product formation. Appl Microbiol Biotechnol 94:1483–1494. https://doi.org/10.1007/s00253-012-4101-5.
18. Heroven AK, Dersch P. 2014. Coregulation of host-adapted metabolism and virulence by pathogenic yersiniae. Front Cell Infect Microbiol 4:146. https://doi.org/10.3389/fcimb.2014.00146.
19. Zhan L, Yang L, Zhou L, Li Y, Gao H, Guo Z, Zhang L, Qin C, Zhou D, Yang R. 2009. Direct and negative regulation of the sycO-ypkA-ypoJ operon by cyclic AMP receptor protein (CRP) in Yersinia pestis. BMC Microbiol 9:178. https://doi.org/10.1186/1471-2180-9-178.
20. Zhan L, Han Y, Yang L, Geng J, Li Y, Gao H, Guo Z, Fan W, Li G, Zhang L, Qin C, Zhou D, Yang R. 2008. The cyclic AMP receptor protein, CRP, is required for both virulence and expression of the minimal CRP regulon in Yersinia pestis biovar microtus. Infect Immun 76:5028–5037. https://doi.org/10.1128/IAI.00370-08.
21. Heroven AK, Sest M, Pisano F, Scheb-Wetzel M, Steinmann R, Bohme K, Klein J, Munch R, Schomburg D, Dersch P. 2012. Crp induces switching of the CsrB and CsrC RNAs in Yersinia pseudotuberculosis and links nutritional status to virulence. Front Cell Infect Microbiol 2:158. https://doi.org/10.3389/fcimb.2012.00158.
22. Liu L, Fang H, Yang H, Zhang Y, Han Y, Zhou D, Yang R. 2016. CRP is an activator of *Yersinia pestis* biofilm formation that operates via a mechanism involving *gmhA* and *waaAE-coaD*. Front Microbiol 7:295. https://doi.org/10.3389/fmicb.2016.00295.
23. Willias SP, Chauhan S, Lo CC, Chain PS, Motin VL. 2015. CRP-mediated carbon catabolite regulation of Yersinia pestis biofilm formation is enhanced by the carbon storage regulator protein, CsrA. PLoS One 10:e0135481. https://doi.org/10.1371/journal.pone.0135481.
24. Aiba H. 1983. Autoregulation of the Escherichia coli crp gene: CRP is a transcriptional repressor for its own gene. Cell 32:141–149. https://doi.org/10.1016/0092-8674(83)90504-4.
25. Gao H, Zhang Y, Yang L, Liu X, Guo Z, Tan Y, Han Y, Huang X, Zhou D, Yang R. 2011. Regulatory effects of cAMP receptor protein (CRP) on porin genes and its own gene in Yersinia pestis. BMC Microbiol 11:40. https://doi.org/10.1186/1471-2180-11-40.
26. Zhang Y, Wang L, Han Y, Yan Y, Tan Y, Zhou L, Cui Y, Du Z, Wang X, Bi Y, Yang H, Song Y, Zhang P, Zhou D, Yang R. 2013. Autoregulation of PhoP/PhoQ and positive regulation of the cyclic AMP receptor protein-cyclic AMP complex by PhoP in Yersinia pestis. J Bacteriol 195:1022–1030. https://doi.org/10.1128/JB.01530-12.
27. Davis KM, Mohammadi S, Isberg RR. 2015. Community behavior and spatial regulation within a bacterial microcolony in deep tissue sites serves to protect against host attack. Cell Host Microbe 17:21–31. https://doi.org/10.1016/j.chom.2014.11.008.
28. de Prost N, Saumon G. 2007. Glucose transport in the lung and its role in liquid movement. Respir Physiol Neurobiol 159:331–337. https://doi.org/10.1016/j.resp.2007.02.014.
29. Pradel E, Lemaitre N, Merchez M, Ricard I, Reboul A, Dewitte A, Sebbane F. 2014. New insights into how Yersinia pestis adapts to its mammalian host during bubonic plague. PLoS Pathog 10:e1004029. https://doi.org/10.1371/journal.ppat.1004029.
30. Ishizuka H, Hanamura A, Inada T, Aiba H. 1994. Mechanism of the down-regulation of cAMP receptor protein by glucose in Escherichia coli: role of autoregulation of the crp gene. EMBO J 13:3077–3082.
31. Steinsiek S, Bettenbrock K. 2012. Glucose transport in Escherichia coli mutant strains with defects in sugar transport systems. J Bacteriol 194:5897–5908. https://doi.org/10.1128/JB.01502-12.
32. Nuss AM, Beckstette M, Pimenova M, Schmuhl C, Opitz W, Pisano F, Heroven AK, Dersch P. 2017. Tissue dual RNA-seq allows fast discovery of infection-specific functions and riboregulators shaping host-pathogen transcriptomes. Proc Natl Acad Sci U S A 114:E791–E800. https://doi.org/10.1073/pnas.1613405114.
33. Sharma P, Khairnar V, Madunic IV, Singh Y, Pandyra A, Salker MS, Koepsell H, Sabolic I, Lang F, Lang PA, Lang KS. 2017. SGLT1 deficiency

turns Listeria infection into a lethal disease in mice. Cell Physiol Biochem 42:1358–1365. https://doi.org/10.1159/000479197.
34. Pechous RD, Broberg CA, Stasulli NM, Miller VL, Goldman WE. 2015. In vivo transcriptional profiling of Yersinia pestis reveals a novel bacterial mediator of pulmonary inflammation. mBio 6:e02302-14. https://doi.org/10.1128/mBio.02302-14.
35. Gill SK, Hui K, Farne H, Garnett JP, Baines DL, Moore LS, Holmes AH, Filloux A, Tregoning JS. 2016. Increased airway glucose increases airway bacterial load in hyperglycaemia. Sci Rep 6:27636. https://doi.org/10.1038/srep27636.
36. Oliveira TL, Candeia-Medeiros N, Cavalcante-Araujo PM, Melo IS, Favaro-Pipi E, Fatima LA, Rocha AA, Goulart LR, Machado UF, Campos RR, Sabino-Silva R. 2016. SGLT1 activity in lung alveolar cells of diabetic rats modulates airway surface liquid glucose concentration and bacterial proliferation. Sci Rep 6:21752. https://doi.org/10.1038/srep21752.
37. Pezzulo AA, Gutierrez J, Duschner KS, McConnell KS, Taft PJ, Ernst SE, Yahr TL, Rahmouni K, Klesney-Tait J, Stoltz DA, Zabner J. 2011. Glucose depletion in the airway surface liquid is essential for sterility of the airways. PLoS One 6:e16166. https://doi.org/10.1371/journal.pone.0016166.
38. Somashekar BS, Amin AG, Rithner CD, Troudt J, Basaraba R, Izzo A, Crick DC, Chatterjee D. 2011. Metabolic profiling of lung granuloma in Mycobacterium tuberculosis infected guinea pigs: ex vivo 1H magic angle spinning NMR studies. J Proteome Res 10:4186–4195. https://doi.org/10.1021/pr2003352.
39. Rempe KA, Hinz AK, Vadyvaloo V. 2012. Hfq regulates biofilm gut blockage that facilitates flea-borne transmission of Yersinia pestis. J Bacteriol 194:2036–2040. https://doi.org/10.1128/JB.06568-11.
40. Choi KH, Gaynor JB, White KG, Lopez C, Bosio CM, Karkhoff-Schweizer RR, Schweizer HP. 2005. A Tn7-based broad-range bacterial cloning and expression system. Nat Methods 2:443–448. https://doi.org/10.1038/nmeth765.
41. Price PA, Jin J, Goldman WE. 2012. Pulmonary infection by Yersinia pestis rapidly establishes a permissive environment for microbial proliferation. Proc Natl Acad Sci U S A 109:3083–3088. https://doi.org/10.1073/pnas.1112729109.
42. Bellows LE, Koestler BJ, Karaba SM, Waters CM, Lathem WW. 2012. Hfq-dependent, co-ordinate control of cyclic diguanylate synthesis and catabolism in the plague pathogen Yersinia pestis. Mol Microbiol 86:661–674. https://doi.org/10.1111/mmi.12011.
43. Schindelin J, Arganda-Carreras I, Frise E, Kaynig V, Longair M, Pietzsch T, Preibisch S, Rueden C, Saalfeld S, Schmid B, Tinevez JY, White DJ, Hartenstein V, Eliceiri K, Tomancak P, Cardona A. 2012. Fiji: an open-source platform for biological-image analysis. Nat Methods 9:676–682. https://doi.org/10.1038/nmeth.2019.
44. Houppert AS, Bohman L, Merritt PM, Cole CB, Caulfield AJ, Lathem WW, Marketon MM. 2013. RfaL is required for Yersinia pestis type III secretion and virulence. Infect Immun 81:1186–1197. https://doi.org/10.1128/IAI.01417-12.